Available online at www.sciencedirect.com
ScienceDirect
Ceramics International 34 (2008) 1509–1520
CERAMICS INTERNATIONAL
www.elsevier.com/locate/ceramint

Microstructure, mechanical and tribological properties of microwave sintered calcia-doped zirconia for biomedical applications

Shekhar Nath, Nikhil Sinha, Bikramjit Basu *

Laboratory for Advanced Ceramics, Department of Materials and Metallurgical Engineering, Indian Institute of Technology, IIT-Kanpur, Kanpur 208016, India

Received 28 July 2006; received in revised form 26 February 2007; accepted 24 April 2007
Available online 15 June 2007

Abstract

Among the available ceramics materials for load bearing bio-implant applications, Y-TZP is superior (fracture toughness: ~10 MPa $m^{0.5}$) for its better mechanical properties. However, due to concerns related to property degradation of Y-TZP during long exposure in body fluid, the current work is taken up to study the feasibility of developing stabilised zirconia ceramics in CaO–ZrO_2 system, using microwave sintering (MW) technique. The present paper reports the processing, microstructure and tribological properties of microwave sintered Ca-doped ZrO_2 based ceramics. An important experimental result is that MW sintering to greater than 90% theoretical density can be achieved in Ca-PSZ (8 mol% CaO) and Ca-FSZ (16 mol% CaO) ceramics by sintering at 1585 °C for 1 h. The sintered materials exhibit Vickers hardness ~8–10 GPa, which would allow them to be used as load bearing implants. Also, a modest fracture toughness (~6 MPa $m^{0.5}$) was measured for Ca-PSZ, which is better than commercial grade alumina. So, it is possible to synthesize a material which has better combination of hardness and toughness than other commercially available bioceramics like alumina, hydroxyapatite, TCP, etc. Considering its specific application for THR (total hip replacement), tribological experiments using fretting wear tester serve to provide data about the wear behaviour of the proposed materials. The fretting experiments were conducted against a bearing-steel counterbody in air as well as in a SBF (simulated body fluid) environment. The wear behaviour of the investigated tribocouple is dominated by the formation of Fe oxide/chloride layer at the worn surface.

Keywords: C. Hardness; Ca-PSZ; Ca-FSZ; Microstructure; Fracture toughness; Tribology; Fretting; Simulated body fluid; Wear rate; Surface profilometry

1. Introduction

Among various structural ceramics, zirconia-based ceramics have been widely researched in the last three decades, because of their better toughness and strength properties [1]. The applications of ZrO_2-based ceramics include mechanical seals, engine components, cutting tools, sensors, and thermal barrier coatings and lately, as biomedical implants [2]. It is known that among the bioceramics, bioinert materials like alumina and zirconia are candidate materials for load bearing implants, e.g. total hip joint replacement (THR), knee joints, etc. [3]. Various combinations of ceramics have been studied for hip joint prostheses, these include alumina on alumina, alumina on zirconia to assess the relative performance/durability in physiological conditions [4]. It was found that the wear rate of Al_2O_3 is ~8 times higher than that ZrO_2 under identical testing conditions [5]. Such high wear resistance for ZrO_2 would evidently ensure longer implant life. It was additionally demonstrated that the presence of zirconia ceramics did not lead to any local or systemic adverse reactions or cytotoxic effects [3].

It is well known that pure monolithic/undoped zirconia has very poor mechanical properties due to volume expansion induced cracking, resulting from the tetragonal to monoclinic ZrO_2 transformation at 1170 °C. CaO, MgO and several other oxides in appropriate amounts are widely used to retain/stabilize the cubic zirconia phase at room temperature. Among stabilized ZrO_2 ceramics, the cubic zirconia phase containing ceramics are widely used for oxygen sensors and as anodes in solid oxide fuel cells [6]. For load bearing biomedical applications, the mechanical properties, in particular hardness and fracture toughness are the important parameters. Until date, yttria stabilized zirconia (Y-TZP) ceramics are popular for biomedical applications due to their high fracture toughness

* Corresponding author. Tel.: +91 5122597771; fax: +91 5122597505.
E-mail address: bikram@iitk.ac.in (B. Basu).

0272-8842/$34.00
doi:10.1016/j.ceramint.2007.04.021

(2Y-TZP: ~10 MPa $m^{0.5}$) [7,8]. In spite of good mechanical properties, Y-TZP materials often behave in unpredictable manner as implants [9]. Such problems have been attributed to the susceptibility of Y-TZPs towards aging induced property degradation. Therefore, other partially and fully stabilized zirconia (CaO, MgO doped) may be used as suitable replacement for Y-TZP and other bioceramics in biomedical applications.

It is now well recognized that the microstructure and properties of ceramics critically depend on processing routes and densification parameters. For partially stabilized zirconia, a high toughness microstructure is generally obtained by sintering, followed by high temperature solid solution treatments for longer time and a controlled cool to room temperature. For example, Wu and Brook [10] densified Ca-PSZ ceramics via conventional sintering in air at 1560 °C for 13 h. They also reported the sintering of Ca-PSZ ceramics at 1700 °C by fast heating using a zone sintering technique. Although such a longer processing time causes extensive grain growth, it helps to precipitate tetragonal phase (often cuboid shaped) in the cubic matrix. It is therefore important to investigate whether the faster heating rate, in combination with shorter sintering time in microwave sintering, can produce microstructure in CaO stabilized ZrO_2 with good material properties, as often obtained by conventional route with a combination of sintering and post-sintering annealing treatment. One of the major aspects of the present work is to address this issue.

For biomedical applications, the tribological properties play an important role, particularly when two similar or dissimilar materials come in contact during applications. For example, in THR application, zirconia ball head is attached with the metallic (Steel/Ti alloys) stent. The joint of these zirconia and metallic part can undergo micro-movement (fretting fatigue) during various external activities. Therefore, it is important to evaluate the material degradation (corrosion, wear) for such type of applications. The evaluation of fretting wear properties of the stabilized ZrO_2s constitutes another goal of the present work.

In order to achieve the above-mentioned objectives, the MW sintering technique is used in the present work for densification of Ca-doped ZrO_2. Controlled sintering of ceramics, by utilizing the microwave has been successfully used to densify Al_2O_3 [11]. The interaction of high frequency electromagnetic fields with polycrystalline dielectric materials leads to volumetric, selective and rapid heating. Since the 1980s, microwave processing of monolith and composite ceramic materials has been recognized to offer a number of advantages over conventional sintering approaches. The increase in densification rate, as well as relatively low sintering temperature and time make the MW fabricating technique significantly faster than the conventional sintering process. Earlier, Upadhaya et al. used MW sintering to densify 3Y-TZP [12] and 9Y-CSZ [13] ceramics. For TZP(Y) 20 wt.% alumina ceramics, a very fine grain (<0.5 μm) structure is obtained after microwave sintering [14]. Interestingly, Xie et al. [15] reported that microwave sintering does not always produce fine-grained ceramic microstructure and in fact, due to rapid diffusion rate grains grow faster during microwave sintering than conventional heating. Based on the above observations, the goal of the present work is to produce calcia-doped zirconia via microwave sintering route. The microstructures as well as the mechanical, tribological properties are characterized.

2. Experimental procedure

2.1. Processing

The ceramic compositions investigated in this study include Ca-PSZ (8 mol% CaO) and Ca-FSZ (16 mol% CaO). Fig. 1 shows the ZrO_2 rich end of the ZrO_2–CaO phase diagram and from this diagram, the composition of investigated materials of the present work has been identified. In this paper, Ca-PSZ will always indicate the material composition of 8 mol% CaO in ZrO_2, whereas Ca-FSZ will indicate the composition of 16 mol% of CaO in ZrO_2, irrespective of the phases present after MW sintering. In order to synthesize Ca-PSZ and Ca-FSZ materials, 8 and 16 mol% CaO is alloyed with monoclinic ZrO_2, respectively. Commercial high purity monoclinic ZrO_2 powder (d_{50} = 7.62 μm, Tosoh TZ-O grade, Japan) was mixed in appropriate proportion with precursor $CaCO_3$ powder (Rankem C0050 grade, India) to obtain a final compositions of 8 and 16 mol% CaO–zirconia ceramics. Because of the use of $CaCO_3$ starting powders, it is expected that the carbonate salt would be decomposed into CaO and CO_2 during calcination/early stage sintering of the mixed powders. The starting powders were mixed on a multidirectional (planetary ball mill) mixer for 24 h in acetone, using tungsten carbide milling balls with powder: balls in 1:5 ratio to break the agglomerates and reduce the particle size further. The mixture thus obtained was calcined at 450 °C for 3 h in air to remove the moisture and other low temperature volatiles. This was followed by cold

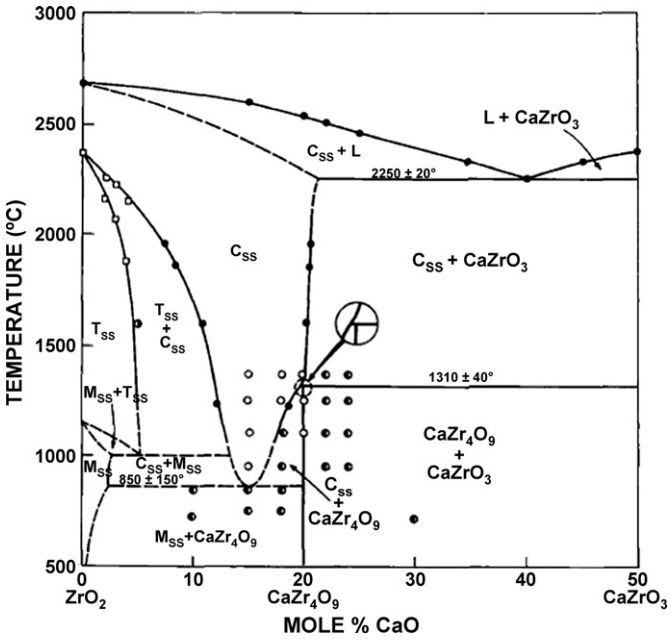

Fig. 1. ZrO_2 rich part of the ZrO_2–CaO binary phase diagram, showing the different phases of ZrO_2 as a function of temperature and mole percent of CaO addition. The details of the phase diagram description can be found in Ref. [32].

uniaxial pressing into pellets of 10 mm diameter using a hydraulic press. Prior to pelletization the calcined powder has the average particle size of ~3 μm (d_{50}), although the particle size varies in the range of 300 nm to 7 μm.

All the Ca-doped zirconia powder mixtures were sintered in a microwave furnace (6 kW, 2.45 GHz, Sinterware, BHEL, India) at selected sintering temperatures of 1500, 1550 and 1585 °C. It is to be noted here that with the present experimental set-up, the maximum possible sintering temperature is 1585 °C. The green samples were placed inside a crucible made of alumina and silicon carbide mixtures. The crucible was covered by alumina wool for insulating purpose in a casket. Silicon carbide acts as susceptor, which at lower temperature absorbs microwave to produce heat. As the microwave absorbing capacity of zirconia is small, at lower temperature the heat absorption by ZrO_2 takes place by radiant heating in the presence of SiC in microwave field, as also reported by earlier researchers [16]. In our experiments, the microwave cavity was operated initially at low electrical power (60% power level) for 20 min, followed by operation at high power (100% power level) for the next 20 min to reach the target temperature. The temperature was measured using an infrared (IR) thermometer. The soaking time at each sintering temperature was 1 h. The samples were allowed to cool by normal casket cooling. The average cooling rate in the temperature range between 1585 and 600 °C was ~15 °C/min for all cases. The density of the sintered samples was measured using water as a fluid, by Archimedes's principle.

2.2. Microstructure and mechanical properties

X-ray diffraction (XRD, model: Rich–Seifert, 2000D) studies were carried out on the sintered and polished surfaces to evaluate the phase assemblages. For microstructural observation, the sintered samples were polished using standard metallographic techniques. The polished sintered samples were thermally etched at a temperature of 100 °C lower than corresponding sintering temperature for 30 min in air to reveal the grain boundaries. The microstructural investigation of the polished and thermally etched specimens was performed using scanning electron microscope (SEM, Quanta FEI). For few samples, SEM images were also taken from the fracture surfaces. The mechanical properties, e.g. hardness measurement were evaluated, using Vickers hardness tester using 10 kg indent load. The indent diagonal length was carefully measured on SEM images of indented surfaces. At 10 kg indent load, cracks were not observed to emanate from the four corners of the indent, and subsequently the samples were indented at higher load (20 kg). Unfortunately, at 20 kg indent load, chipping occurred from the indent sides, and therefore, the indentation data were not used to calculate fracture toughness for most of the sintered samples. Only in the case of 8 mol% Ca-PSZ sample (sintered at 1585 °C), well-defined radial/median cracks were observed from the indent corners. The indentation toughness was measured by Anstis et al. formula [17] after carefully measuring the crack lengths from high magnification SEM images of indented surface.

2.3. Tribological properties evaluation

The tribological (fretting) behavior of the Ca-PSZ and FSZ were evaluated using a ball-on-flat fretting wear tester (DUCOM, Bangalore, India) [18]. The polished Ca-PSZ/FSZ samples, sintered at different temperature, were used as flat (reciprocating motion) materials and a commercial steel ball (stationary) as a counterbody. A 6 mm diameter bearing grade (commercial SAE 52100 grade) steel ball was used as the moving counterbody. The friction and wear behavior of the MW sintered materials were compared with the previously reported Y-TZP materials, which is an important biomaterial used in total hip joint replacement (THR) assembly. The commercial THR assembly consists of a femoral head made of Y-TZP/alumina. 'Fretting' is defined as low amplitude (of ~80 μm, one-way travel length) reciprocatory tangential sliding. It can be noted that majority of the wear tests of biomaterial combinations are subjected to standard reciprocating motion similar to real contact conditions prevalent in the human body. An inductive displacement transducer monitored the displacement of the flat sample. The friction force was recorded with a piezoelectric transducer attached to the holder that supports the counterbody. The friction coefficient was obtained from the on-line measured tangential force.

Prior to the fretting tests, both the flat and ball were ultrasonically cleaned in acetone. All the fretting experiments were conducted at temperature of (35 ± 2 °C) with relative humidity (RH) of 45 ± 5% as well as in simulated body fluid (SBF). To carry out the experiments in SBF, the test plate with the sample was placed in the testing rig, completely filled with SBF solution (Hank's solution [19]). In order to investigate the severe wear behavior, the wear tests were performed at 10 N normal load. All the tests were performed for 10^5 cycles with relative displacement stroke between the flat and ball set to 80 μm and the frequency at 10 Hz (see Fig. 2). This combination of testing parameters resulted in a gross slip fretting contact. The electrolyte used for simulating human body fluid conditions was Hank's balanced electrolyte salt solution, which was prepared using laboratory grade chemicals and double distilled water. The composition of Hank's balanced salt solution used was (values in g/l) 8NaCl, 0.4KCl, 0.14$CaCl_2$,

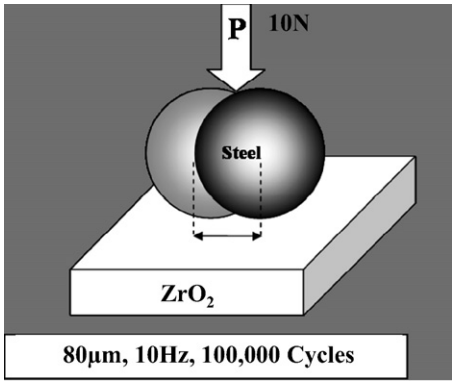

Fig. 2. Schematic representation of fretting mode I (ball-on-flat configuration) test, showing experimental fretting parameters for Ca-PSZ/FSZ samples against bearing steel ball. Here the half cycle travel length is 80 μm.

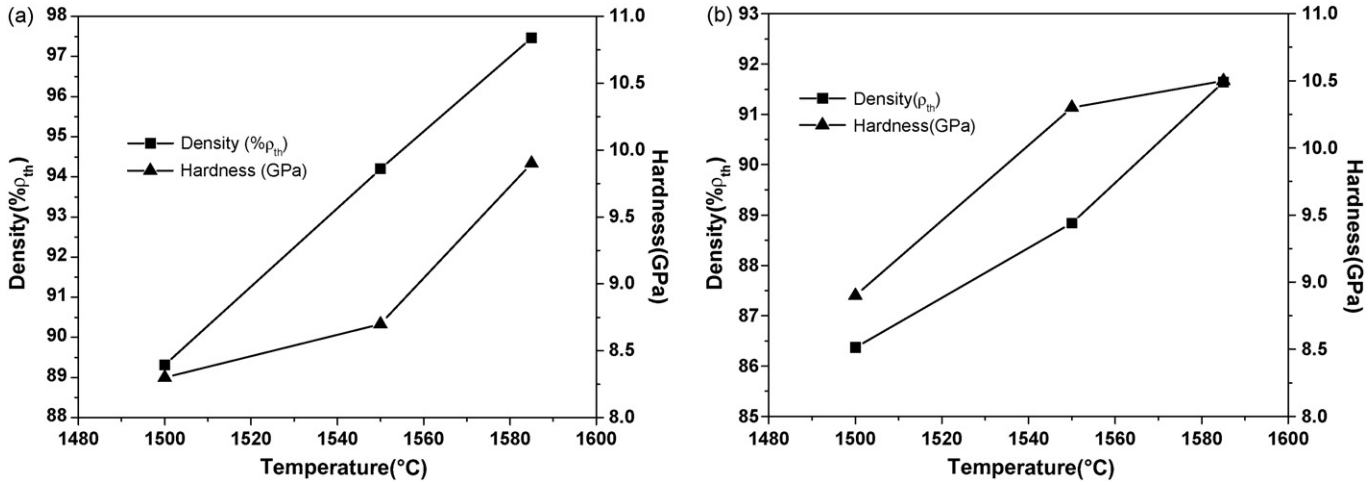

Fig. 3. Variation of hardness and density of microwave sintered (a) Ca-PSZ and (b) Ca-FSZ as a function of sintering temperature.

$0.06MgSO_4{\cdot}7H_2O$, $0.06NaH_2PO_4{\cdot}2H_2O$, $0.35NaHCO_3$, 1.00 glucose, $0.06KH_2PO_4$, and $0.10MgCl_2{\cdot}6H_2O$. The pH of the freshly prepared SBF solution was precisely maintained at 7.4. Freshly prepared solution was used for each experiment. The accuracy of the temperature and humidity maintained in this investigation was ±2 °C and ±5%, respectively. These parameters were maintained by placing the fretting wear tester in an environmental chamber, provided with temperature and humidity control. The wear volumes of the samples were determined from the measured wear scar diameters as per the equation given by Klaffke [20]. The use of this equation is reported to be justified for the present fretting conditions (providing errors less than 5%) when the wear scar diameter is larger than twice the Hertzian contact diameter, as was the case in our experiments. From the estimated wear volume, the specific wear rates (wear volume/(load × distance)) were calculated. Further detailed characterization of the worn surfaces was done using a scanning electron microscope, SEM (Philips, Quanta-FEI). The compositional analysis of the tribolayer is carried out by EDS, attached with SEM. Also, the worn surfaces were scanned under a Laser Surface Profilometer (Mahr GmbH, Germany) to determine the profile depth.

3. Results and discussion

3.1. Densification and phase assemblage

The density data, presented in Fig. 3a and b reveals that the sintered density of both Ca-PSZ and Ca-FSZ monotonically increases with MW sintering temperature, reaching a maximum density at 1585 °C. However, the maximum density achieved in Ca-PSZ (∼97.5% ρ_{th}) is more when compared with Ca-FSZ (∼91.6% ρ_{th}). It can be mentioned here that the formation of oxygen vacancies takes place due to CaO doping:

$$CaO \overset{ZrO_2}{\rightleftarrows} Ca''_{Zr} + O_o{}^{x} + V_o{}^{\infty}$$

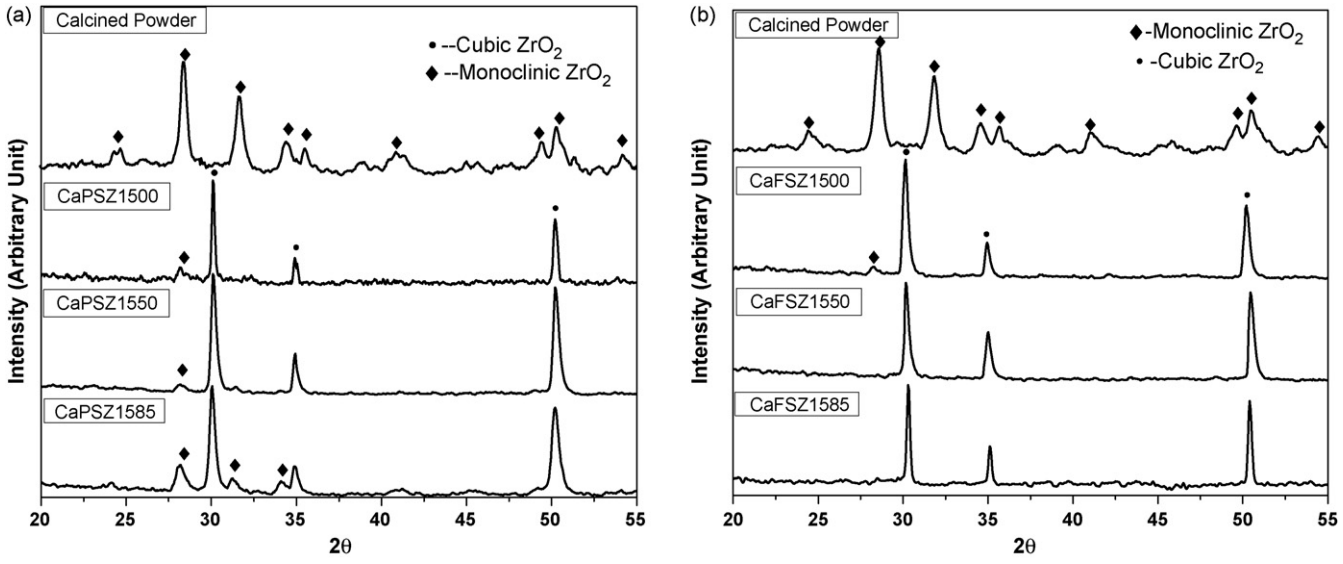

Fig. 4. X-ray diffraction spectra, acquired from polished surfaces of Ca-PSZ (a) and Ca-FSZ (b), after microwave sintering at various temperatures for 1 h.

The densification kinetics of doped ZrO_2 therefore is determined by oxygen vacancy diffusion with the rate-limiting step being the diffusion of cations. Therefore, it is expected that the sluggish mass transport rate to the neck region, at higher dopant content, can potentially cause poor densification in 16 mol% Ca-doped zirconia. At higher CaO content, the decrease in densification can also be attributed to the trapping of oxygen vacancies by the formation of defect associates, which lead to a decrease in concentration of free oxygen vacancies. Although the densification kinetics depends on the particle size and surface area of the starting powders as well as on green density (being similar for both the studied samples); it is to be pointed out here that the aspect related to particle size/surface area has not been critically assessed in the present work. In an earlier work, Upadhaya et al. [13] observed the beneficial effect of microwave radiation in sintering of cubic zirconia materials. It was reported there that the rapid sintering kinetics is due to the dielectric heating as well as the field-enhanced mobility during diffusion. It can be mentioned here that sintering of yttria stabilized cubic zirconia in microwave route at 1625 °C for 35 min have yielded upto 97% densification [13]. Also, the sintering of 15 mol% calcia-doped zirconia (with 1 mol% alumina) at 1600 °C (for 4 h) has been reported to result in a density of 5.44 g/cm^3 (98% ρ_{th}) [21]. From the above observations, it is evident that Ca-doped ZrO_2 can be sintered using a microwave sintering technique, to more than 90% theoretical density at comparable temperature with conventional sintering, but at a much faster rate, i.e. in shorter time.

XRD spectra acquired from the sintered and polished surfaces of Ca-PSZ and Ca-FSZ are shown in Fig. 4a and b. Overall, the variation in microwave sintering temperature has more noticeable influence on the phase assemblage of Ca-PSZ ceramics, in comparison with that of Ca-FSZ materials. The analysis of the XRD peaks reveals that the Ca-PSZ materials predominantly contain cubic ZrO_2 (JCPDS file no. 27-0997) with small amount of m-ZrO_2 (JCPDS file no. 37-1484). The m-ZrO_2 content in Ca-PSZ appears to be more in case of samples sintered at 1585 °C. The reason for this anomalous result is still not known. Garvie et al. [1] described to differentiate tetragonal phase with cubic phase using XRD pattern. For this purpose, XRD patterns of PSZ samples (1550 and 1585 °C samples) in the 2θ range of ~72°–75° are presented in Fig. 5 and compared with the result obtained by Garvie et al. [1]. This comparison shows that reflection from cubic (4 0 0) plane is present, whether reflection from tetragonal (0 0 4) and (2 2 0) are absent in the present case. Therefore, the presence of tetragonal phase in PSZ samples can be ruled out. In case of Ca-FSZ materials, only traces of m-ZrO_2 are detected after microwave sintering at 1500 °C. However, after MW sintering at 1550 °C or higher temperature, the Ca-FSZ materials contain only cubic-ZrO_2. Similar to PSZ samples, there are no peaks found corresponding to tetragonal phase, in the 2θ range of ~72°–75° (not shown) for FSZ samples.

For better understanding the phase assemblage in the sintered compact needs to be explained. Observing the ZrO_2–CaO binary phase diagram (Fig. 1), it appears that sintering for 8CaO-doped zirconia occurs in the two-phase (t + c) phase field

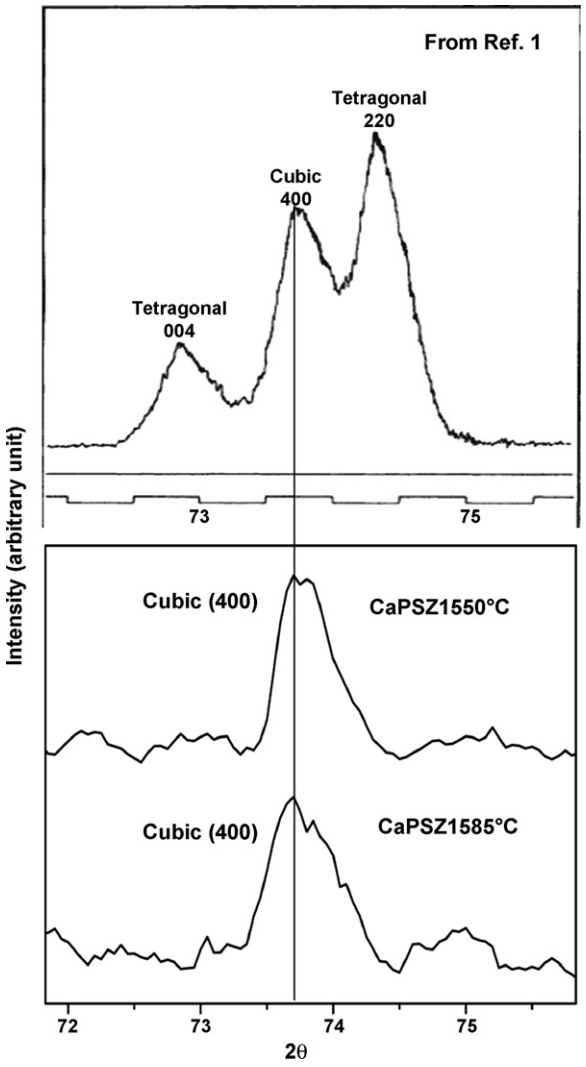

Fig. 5. X-ray spectra collected at the range of ~72–75° (2θ value) for PSZ samples sintered at 1550 and 1585 °C for 1 h and the results are compared with the XRD pattern, obtained with Ca-stabilized zirconia using Cu Kα radiation (result extracted from Ref. [1], top graph). This comparison shows the absence of tetragonal phase for PSZ samples, when sintered in MW furnace. Similar result was also obtained with FSZ samples.

and the slow cooling (normal casket/furnace cooling) of such composition will lead to the phase assemblage of (c + m) at a temperature of 1000 °C or lower. In the present case, the post-fabrication cooling in the microwave casket also leads to (c + m)-two phase microstructure for 8CaO-doped zirconia. This is probably due to the nature of cooling in microwave casket, which is possibly slower cooling. However, for 16CaO-doped zirconia, all the sintering experiments are carried out in the cubic phase field, according to ZrO_2–CaO equilibrium diagram. The microstructural analysis also confirms the retention of the predominant cubic phase.

3.2. Microstructure and mechanical properties

Some representative SEM images of the microwave-sintered microstructures are presented in Fig. 6a and b. In case of Ca-PSZ sample (polished and thermally etched surfaces), an

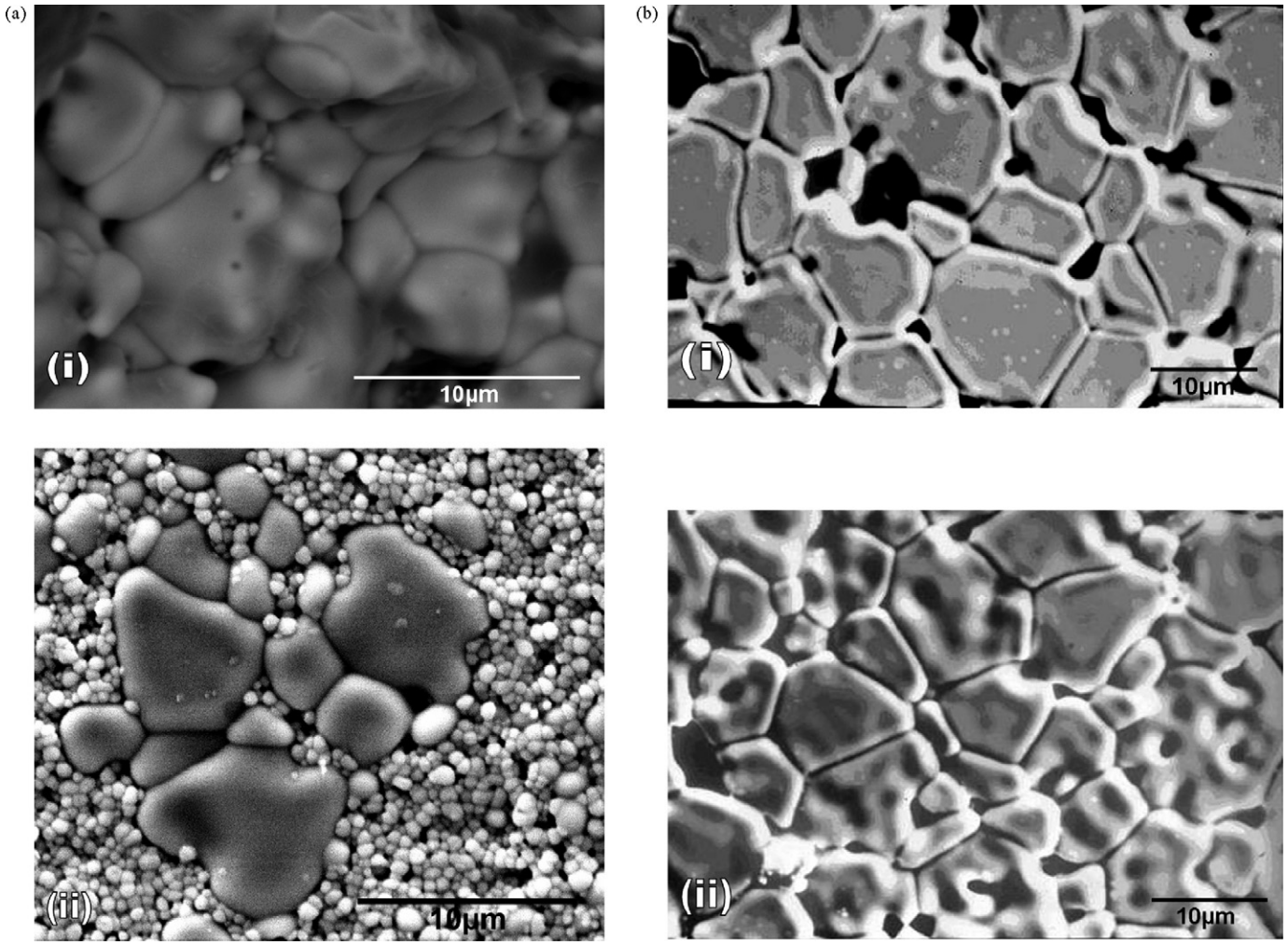

Fig. 6. (a) Representative SEM images of fracture surface of (i) Ca-PSZ (MW, 1585 °C) showing intergranular fracture, (ii) polished and thermally etched Ca-PSZ (MW, 1585 °C). (b) Representative SEM images of polished and thermally etched of Ca-FSZ ceramic: MW sintered at (i) 1550 °C and (ii) 1585 °C.

interesting observation is that coarser m-ZrO_2 grains (∼10 μm) are embedded in a rather finer c-ZrO_2 microstructure (Fig. 6a(ii)). High magnification SEM image (Fig. 6a(i)) of the fracture surface reveals the presence of non-equiaxed grains of coarser m-ZrO_2. Such bimodal grain size of Ca-PSZ can be expected in two-phase microstructure, as also explained earlier. Correlating with the XRD results, it is therefore confirmed that the coarser grains are monoclinic ZrO_2 phase, which are embedded in a finer cubic matrix. The observation of such a heterogeneous microstructure with coarser phase also indicates that microwave sintering is not always capable of producing finer microstructure in specific ceramic system.

In case of Ca-FSZ samples, two representative SEM images of the samples, sintered at 1550 and 1585 °C are provided (Fig. 6b(i and ii)). The grain size measurement using image-pro software reveals that the average grain size is around 7.4 μm with some coarse grain of upto 10–15 μm. The sizes of the grains are comparable for both 1550 and 1585 °C sintered FSZ materials. Observing the size and number of pores, it is clear that while the density increases with sintering temperature, some of the finer pores remain within the grains or trapped at the grain boundary. The pore size in Ca-FSZ sintered at 1585 °C, is finer (submicron) and upto around 2–3 μm in Ca-FSZ, sintered at 1550 °C. Some grain pullouts also are observed in case of 1550 °C sintered FSZ sample, which may occur during ceramographic sample preparation. Another observation is that the grain boundaries are well faceted in the Ca FSZ materials. From the fracture surface of the PSZ samples, it is clear that the dominant mechanism is intergranular type of fracture. For biomedical applications, the presence of micro-pores will allow better anchorage with surrounding cells and thus improve the mechanical attachment of these materials during initial period of implantation [22]. However, it has been reported that the micropores do not have any long-term advantage in terms of biocompatibility of the materials [22].

The mechanical properties of the two compositions (8 mol% CaO and 16 mol% CaO) are summarized in Fig. 3a and b. The variation of hardness and density with sintering temperature is also plotted in Fig. 3. From the data in Fig. 3, it can be commented that the increase in hardness and density of these ceramics commensurate well with each other. Furthermore, the Vickers hardness of the sintered ceramics was found to be of 9.9 and 10.5 GPa for the PSZ and FSZ samples, respectively. Although the density of PSZ materials are higher than the FSZ

samples, but the FSZ materials posses better hardness than PSZ samples. This is due to the fact that monoclinic zirconia is considerably softer than the c- or t-phases and because of that the less dense single phase FSZ is harder than the two-phase PSZ sample. Such superior hardness is of added advantage over other conventional implant materials, like steel. As mentioned in the experimental section, the cracks around indents are not observed at 10 kg indent load. However, upon increasing load to 20 kg, well-developed cracks with clear indent are observed only in Ca-PSZ (1585 °C). The fracture toughness of PSZ sample sintered at 1585 °C is around 6 MPa $m^{0.5}$, which is not as high as Y-TZP (∼10 MPa $m^{0.5}$) [7,8], but higher than alumina ceramics (K_{IC} ∼3–4 MPa $m^{0.5}$).

3.3. Friction and wear properties

The tribological experiments were carried out on optimized Ca-PSZ (MW, 1585 °C) and Ca-FSZ (MW, 1585 °C) in air as well as in SBF environment and the COF plots are provided in Fig. 7. COF increases to a high value in running in period (first 1000–3000 cycles) and subsequently attains a steady-state value. Also, the frictional behavior of the investigated tribocouple at the load of 10 N is stable as can be noted by the absence of any observable fluctuation in the friction plot. The data in Fig. 7 clearly indicates that steady-state COF is closer to about 0.5, irrespective of the tribological environment (air/SBF). Therefore, it can be assumed that the SBF solution does not provide much lubrication effect in case of stabilized ZrO_2–steel combination. Kalin et al. [23] studied the effect of lubrication (different pH solution) for zirconia as a function of friction and wear properties. At pH of 8 (solution), the COF was around 0.8 and the wear mechanism involved the formation of tribochemically assisted wear-debris layers. Such layers were subsequently spalled and thereby, resulted in rough surfaces with very high wear and high friction.

The wear volumes of worn ZrO_2 are computed by measuring the wear scar diameter in the transverse direction on the as fretted samples and following the Klaffke's equation [20].

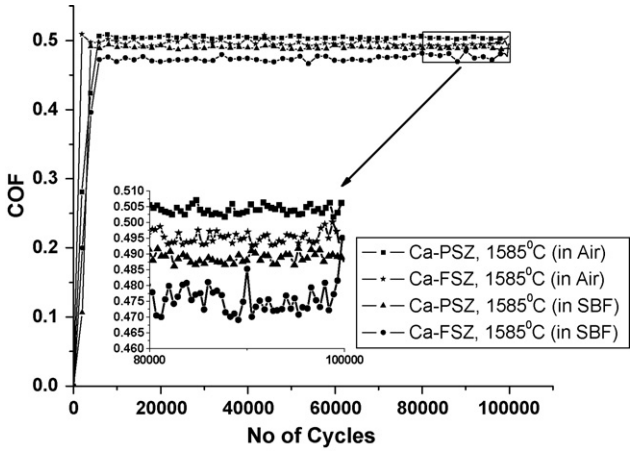

Fig. 7. Plot of coefficient of friction (COF) vs. number of fretting cycles for various investigated Ca-doped zirconia against bearing steel. The difference in steady-state COF at the last phase of testing period is shown as inset.

Table 1
Wear rate and wear volume of two selected (the most densified sample from each group) Ca-doped zirconia, fretted in air and SBF against bearing steel ball

Sample details	Experimental environment	Wear rate (mm^3/N m)	Maximum wear depth (μm)
Ca PSZ 1585 °C, 1 h	Air	5.3×10^{-5}	10
Ca FSZ 1585 °C, 1 h	Air	4.1×10^{-5}	5
Ca PSZ 1585 °C, 1 h	SBF	3.4×10^{-6}	7
Ca FSZ 1585 °C, 1 h	SBF	4.1×10^{-7}	3

Table 1 displays the wear rate and maximum wear depth for PSZ and FSZ samples, fretted in air as well as in SBF. The wear rate varies in the order of 10^{-5} to 10^{-7} mm^3/N m, depending on tribological environment. Also, the wear rate is more after fretting in air, with higher wear recorded for Ca-PSZ. In case of fretting in SBF solution, lower wear is measured for Ca-FSZ material. 2D surface profiles of worn surfaces were acquired using Laser Surface Profilometer and representative scans are illustrated in Fig. 8. The wear depth data also confirms more severity of wear in air than in SBF environment. It can be noted that for Ca-FSZ, a much lower depth of less than 3 μm is recorded after fretting in SBF.

The evaluation of tribological properties of Ca-doped ZrO_2/steel couple needs to be assessed in the light of earlier published research results. Campbell et al. [24] investigated the fretting wear behavior of selected ceramics and cermets, including zirconia-toughened alumina (ZTA). They recorded COF value of around 0.6–0.7 for ZTA against Cr–steel ball using ball-on-disc fretting wear tester, after 50,000 cycles with

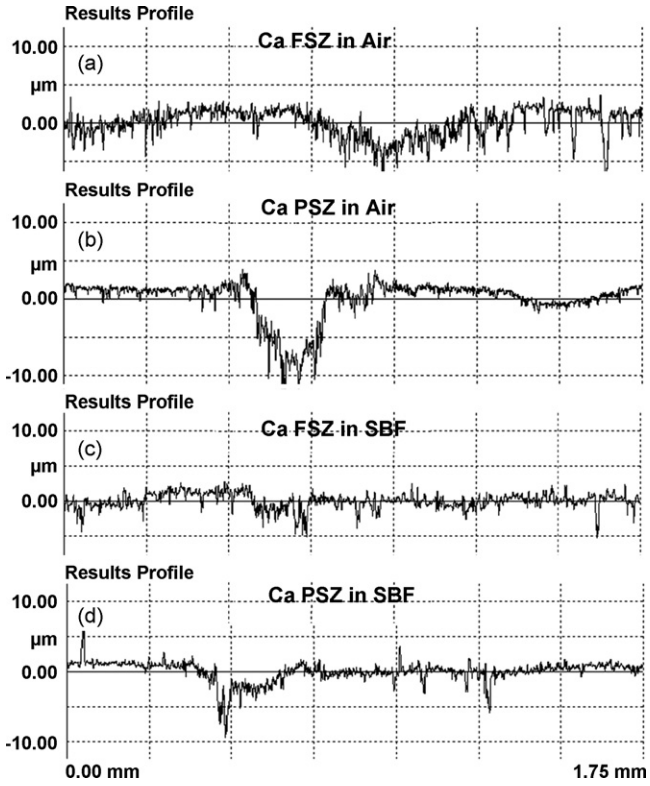

Fig. 8. 2D surface profiles of worn surfaces on various investigated materials after testing against steel in air/SBF environment.

1 N load. Sun et al. [25] reported the unlubricated friction and wear behavior of zirconia ceramics. In their experiments, 12Ce-TZP/10 mol% Al_2O_3 and 12Ce-TZP ceramics against bearing steel were investigated by block-on-ring tribometer at room temperature. COF values were in the range of 0.5–0.7, depending on normal loads. Wang et al. [26] investigated the wear properties of lubricated PSZ materials and compared the results with unlubricated condition. In unlubricated condition, the COF is around 0.4 and the wear rate is in the order of 10^{-5} mm^3/N m for pin-on-disc tribopair in sliding experiments. Chen et al. [27] performed the sliding wear test on PSZ materials (pin) against steel (disc) at different sliding speed and they recorded severe wear rate of 10^{-4} mm^3/N m (linear pin wear rate) with 5 N load. Stachowiak et al. [28] studied the wear properties of Mg-PSZ and Y-TZP on pin-on-disc sliding tester. The self-mated Mg-PSZ and Y-TZP had maximum COF of 0.62 and 0.69, respectively, whereas COF against cast iron was 0.44 (Mg-PSZ) and 0.47 (Y-TZP). In another work, the same group of researchers studied the fretting wear of PSZ (9.6 mol% MgO) against steel ball and recorded COF of 0.5 at 5 N load [29]. In a different work, Klaffke [20] reported the COF of ZrO_2 (doped with 3.3 wt.% MgO) against steel ball to be around 0.55 at humidity level of 50% RH. Also, the wear rate is in the range of 10^{-5} mm^3/N m at dry fretting condition with a wear depth of around 10 μm. In another investigation, Hannink et al. [30] described PSZ ceramic as a good material for tribological applications due to its better combination of mechanical properties than other available ceramics. In case of

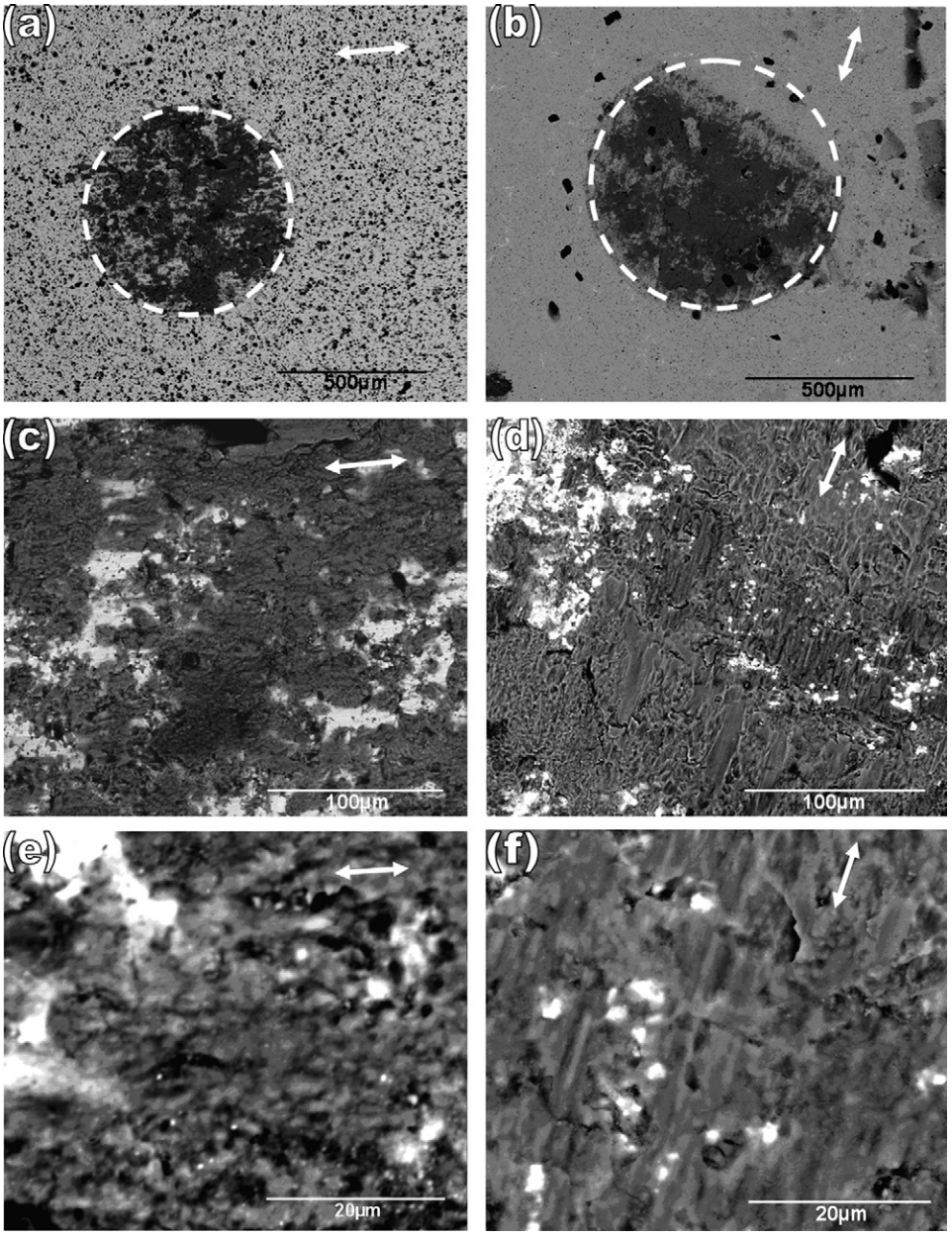

Fig. 9. SEM images of worn surfaces on Ca-FSZ ceramics (MW, 1585 °C) (a, c and e) and that on Ca-PSZ ceramic (b, d and f) after testing against steel in air. The double pointed arrow indicates fretting direction. In (a) and (b) the white circles show the wear scar after fretting in ambient environment. Fretting conditions: 10^5 cycles, 10 Hz frequency, 10 N load and 80 μm stroke length. Counterbody: 6 mm diameter steel ball.

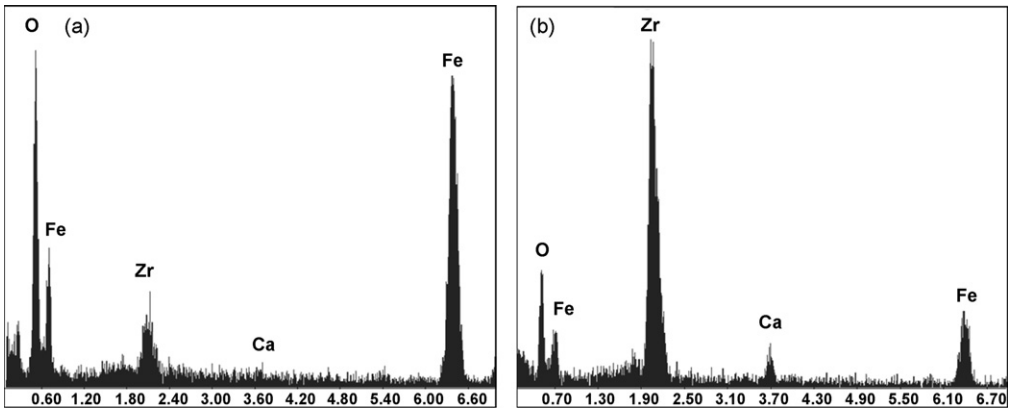

Fig. 10. EDS analysis of the regions within the wear scars show (a) dark contrast region and (b) brighter contrast region of worn surfaces (see Fig. 9c–f) on Ca-FSZ after testing in air. Similar EDS analysis has also been obtained from the worn Ca-PSZ surface.

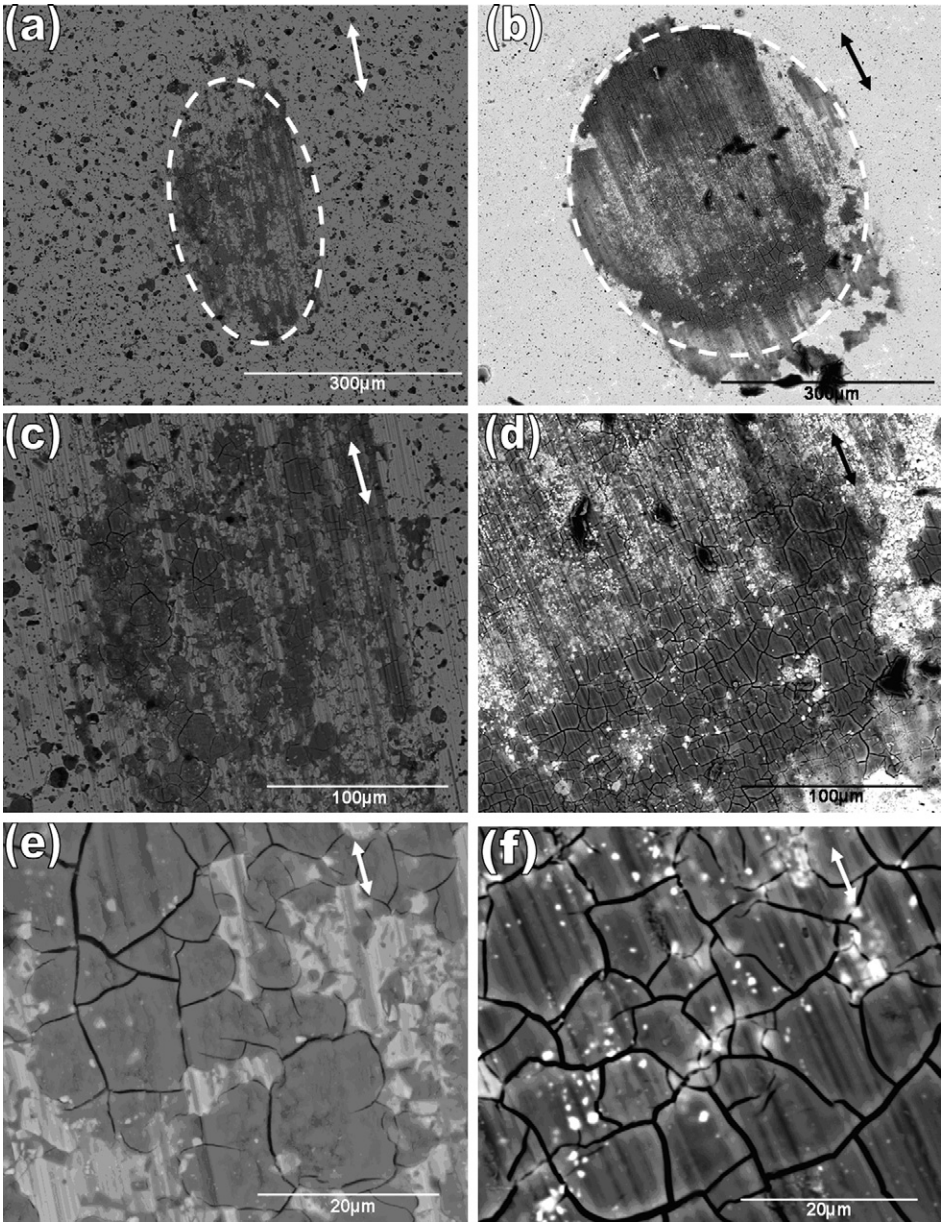

Fig. 11. SEM images of worn surfaces of Ca-FSZ ceramics (MW, 1585 °C) (a, c, and e) and that on Ca-PSZ ceramic (b, d, and f) after testing against steel in SBF. In (a) and (b) the white ellipses show the wear scar after fretting in SBF medium. The cracks are prominent in the tribolayer presented in (e) and (f). The double pointed arrow indicates fretting direction. Fretting conditions: 10^5 cycles, 10 Hz frequency, 10 N load and 80 μm stroke length. Counterbody: 6 mm diameter steel ball.

self-mated PSZ at very low sliding speed, they measured wear rate of 10^{-7} to 10^{-8} $mm^3/N\ m$ and for PSZ-metal pair the COF was around ~0.5. From the above discussion, it should be clear that the microwave sintering of CaO-doped ZrO_2 ceramics provide us with sintered materials of comparable tribological properties.

3.4. Wear mechanisms

Detailed SEM-EDS analyses of the worn surfaces were carried out to understand the wear mechanism and tribolayer formation. Some representative SEM-EDS analyses of the wear scars for PSZ and FSZ samples are presented in Figs. 9–12. Observing Figs. 9 and 11, some salient features can be summarized: (a) under identical fretting conditions, the investigated ceramic exhibit better wear resistance in SBF, compared to that in air; however steady-state COF remains almost similar and (b) irrespective of testing in air/SBF environment, wear damage zone are commonly covered with a tribochemical layer. EDS compositional analysis (Fig. 10) indicates that the darker contrast tribolayer is Fe-oxide rich as much stronger O-peak, compared to that from underlying brighter contrast region, is recorded. Several tiny microcracks are observed on the tribolayer and the fragmentation of such layer is commonly observed.

In case of fretting in SBF solution, the wear scar is of elliptical shape along the fretting direction with the transfer layer/tribolayer being smeared on the fretted surface (Fig. 11). It is to be noted here that elliptical shaped wear scar indicates very low wear rate. In case of higher wear rate (like dry condition), the contact no longer remains point contact and hence the transverse radius of wear scar becomes larger, culminating circular wear scar. Further investigation by higher magnification SEM observations indicates very thin nature and extensive cracking of tribochemical layer. The presence of abrasive scratches is also noticed. Based on the SEM-EDS observation (Figs. 11 and 12) it is clear that tribochemical layer is rich in Fe, O and Cl after testing in SBF solution. Although the severe cracking is noticed on tribochemical layer, such cracking is believed to have developed during drying after testing in SBF. From the physics of the tribological interaction between steel ball and ZrO_2 flat in different environment (air/SBF), the following tribochemical/oxidative reactions are proposed:

$$4Fe + 3O_2(g) = 2Fe_2O_3 \quad (air/SBF) \tag{1}$$

$$3Fe + 2O_2(g) = Fe_3O_4 \quad (air/SBF) \tag{2}$$

$$Fe_2O_3 + 3H_2O = 2Fe(OH)_3 \quad (air/SBF) \tag{3}$$

$$4Fe + 12NaCl + 3O_2(g) = 4FeCl_3 + 6Na_2O \quad (SBF) \tag{4}$$

$$4Fe + 12KCl + 3O_2(g) = 4FeCl_3 + 6K_2O \quad (SBF) \tag{5}$$

$$4Fe + 6CaCl_2 + 3O_2(g) = 4FeCl_3 + 6CaO \quad (SBF) \tag{6}$$

$$4Fe + 12NaCl + 6H_2O + 3O_2(g) = 4FeCl_3 + 12NaOH \quad (SBF) \tag{7}$$

$$4Fe + 12KCl + 6H_2O + 3O_2(g) = 4FeCl_3 + 12KOH \quad (SBF) \tag{8}$$

$$4Fe + 6CaCl_2 + 6H_2O + 3O_2(g) = 4FeCl_3 + 6Ca(OH)_2 \quad (SBF) \tag{9}$$

Based on the available thermodynamic data [31], the free energy change for each reaction occurring from left to right (ΔG) is calculated. The calculated ΔG data for all the above reactions is plotted against temperature in Fig. 13. Observing data in Fig. 13, it should be evident that only reactions (1), (2), and (6)–(9) are thermodynamically feasible in the range of room temperature (RT) to 1200 °C. It has been widely recognized that the contact temperature (bulk and flash), generated due to frictional heating plays an important role in determining the nature of tribochemical reactions. Although the contact temperature for the investigated tribocouple has not been calculated in the present work, the fact that ΔG for selected reactions are negative in a wider temperature range (RT—1200 °C), indicates the clear possibility of their occurrence during fretting wear.

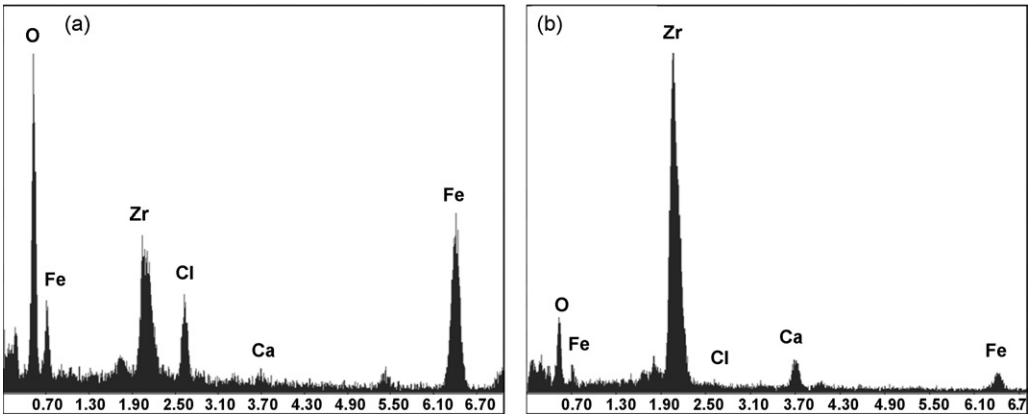

Fig. 12. EDS analysis of the regions within the wear scars show (a) dark contrast region and (b) brighter contrast region of worn surfaces (see Fig. 10c–f) on Ca-FSZ after testing in SBF. Similar EDS analysis has also been recorded from worn Ca-PSZ surface.

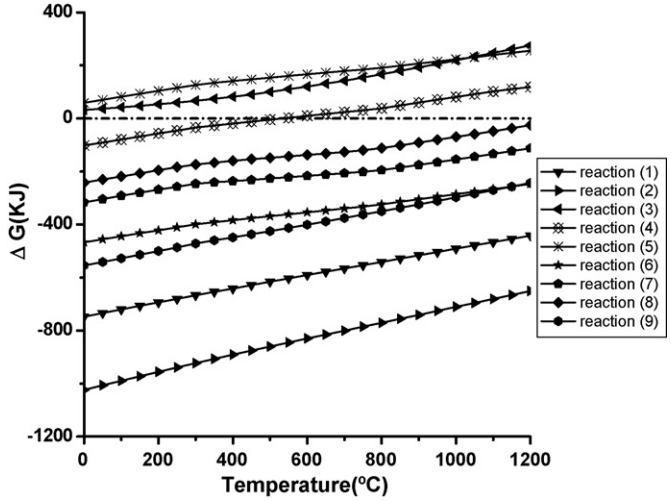

Fig. 13. Plot of free energy change (ΔG) values vs. temperature for different proposed reactions.

Critical observation of the thermodynamic data, as plotted in Fig. 13 provides us with some indication about the relative feasibility among the competing tribochemical reactions. As far as the Fe-oxidation during the initial stages of fretting is concerned, reaction (2) appears to be more thermodynamically feasible and therefore Fe_3O_4 (relative to Fe_2O_3) formation is favored. As far as the formation of chlorides is concerned, the reactions (6)–(9) are feasible. However, because of more negative free energy change, both reactions (6) and (9) are thermodynamically more favored than reactions (7) and (8).

Summarizing the wear mechanisms, it is clear that the tribochemical reactions, leading to the formation of Fe_3O_4- and Fe_2O_3- rich layer occurs during the fretting process. The presence of such layer at the fretting interface, can protect the underneath zirconia sample from further wear, which leads to high wear resistance of Ca-doped ZrO_2 against steel counter body. However, once the steady state is attained, the contact is established between steel ball and (Fe_xO_y, $FeCl_3$)-rich tribochemical layer in all cases and therefore, a constant COF of 0.5 is recorded.

4. Summary and conclusions

(a) Microwave sintering experiments in the temperature range of 1500–1585 °C, reveal that 8 mol% CaO-doped PSZ ceramics with 97.5% ρ_{th} and 16 mol% CaO-doped FSZ with 91.6% ρ_{th} can be obtained after sintering at 1585 °C for 1 h. The density and hardness property increases with increase in sintering temperature.

(b) The microstructure of Ca-PSZ ceramic is characterized by bimodal grain size distribution of coarser m-ZrO_2 grains, embedded in cubic matrix. However, the microstructure of Ca-FSZ contains predominantly c-ZrO_2 phase. The fracture surface reveals that the intergranular fracture is the dominant fracture mechanism.

(c) The optimized Ca-PSZ and Ca-FSZ ceramics exhibit Vickers hardness of around 10 and 9 GPa, respectively. Such superior hardness, compared to that of steel (5–7 GPa) can be exploited in load bearing implant applications. The toughness was measured for Ca-PSZ, as 6 MPa $m^{0.5}$, which is a higher value than other bioceramics, like alumina.

(d) Irrespective of material composition, similar frictional behavior is recorded under both the fretting conditions (air and SBF). A steady-state COF of ~0.5 against bearing steel ball is measured. The wear mechanism is dominated by the formation of Fe_xO_y-rich tribochemical layer, which was in contact with steel counterbody after the steady state is attained. In case of SBF medium, such tribochemical layer additionally contains $FeCl_3$ and the formation of such tribochemical product has been explained on the basis of a number of thermodynamically feasible reactions with SBF.

(e) The investigated materials experience wear rate in the order of 10^{-5} mm^3/N m (in air) and 10^{-6} to 10^{-7} mm^3/N m (in SBF) with the lowest wear rate recorded with FSZ materials in SBF solution. The maximum wear depth is ~3–10 μm, with the highest measured for Ca-PSZ, after fretting in air.

(f) From SEM-EDS investigation of the topography of worn surfaces, it can be inferred that a combination of abrasive, adhesive and tribochemical wear (Fe_2O_3/Fe_3O_4 and $FeCl_3$ layer) play a major role to protect the underneath materials (MW-sintered Ca-PSZ/Ca-FSZ) from fretting damage. The tribochemical layers appear to form on abraded surface and thereby, reduce the material damage from continued wear process.

References

[1] R.C. Garvie, R.H. Hannink, R.T. Pascoe, Ceramic steel? Nature 258 (1975) 703–704.
[2] http://www.accuratus.com/zirc.html.
[3] C. Piconi, G. Maccauro, Zirconia as a ceramic biomaterial, Biomaterials 20 (1999) 1–25.
[4] M. Ueno, K. Ikeichi, Investigation of the wear properties of ceramic total hip prostheses made of alumina and zirconia combination: a hip simulato study, Key Eng. Mater. 240–242 (2003) 809–812.
[5] C. Chung, T. Yang, W. Cheng, J. Wei, Effects of material properties and testing parameters on wear properties of fine-grain zirconia (TZP), Wear 242 (2000) 97–104.
[6] M.A. Janney, C.L. Calhoun, H.D. Kimrey, Microwave sintering of solid oxide fuel cell materials. I. Zirconia–8 mol% yttria, J. Am. Ceram. Soc. 75 (2) (1992) 341–346.
[7] N. Gupta, P. Mallik, B. Basu, Y-TZP ceramics with optimized toughness: new results, J. Alloys Compd. 379 (2004) 228–232.
[8] B. Basu, J. Vleugels, O. Van Der Biest, Y-TZP ceramics with tailored toughness, Key Eng. Mater. 206–213 (2002) 1185–1188.
[9] Website address: http://www.prozyr.com/.
[10] S.X. Wu, R.J. Brook, Kinetics of densification in stabilized zirconia, Solid State Ionics 14 (1984) 123–130.
[11] M. Mizuno, S. Obata, S. Takayama, S. Ito, N. Kato, T. Hirai, M. Sato, Sintering of alumina by 2.45 GHz microwave heating, J. Eur. Ceram. Soc. 24 (2004) 387–391.
[12] D.D. Upadhaya, A. Ghosh, K.R. Gurumurthy, R. Prasad, Microwave sintering of zirconia ceramics, J. Mater. Sci. 36 (2001) 4707–4710.
[13] D.D. Upadhaya, A. Ghosh, K.R. Gurumurthy, R. Prasad, Microwave sintering of cubic zirconia, Ceram. Int. 27 (2001) 415–418.
[14] N.A. Travitzky, A. Goldstein, O. Avsian, A. Singurindi, Microwave sintering and mechanical properties of Y-TZP: 20 wt.% Al_2O_3 composites, Mater. Sci. Eng. A 286 (2000) 225–229.

[15] Z. Xie, J. Yang, Y. Huang, Densification and grain growth of alumina by microwave processing, Mater. Lett. 37 (1998) 215–220.
[16] P.D. Ramesh, D. Brandon, L. Schachter, Use of partially oxidized SiC particle bed for microwave sintering of low loss ceramics, Mater. Sci. Eng. A 266 (1999) 211–220.
[17] G.R. Anstis, P. Chantikul, B.R. Lawn, D.B. Marshall, A critical evaluation of indentation techniques for measuring fracture toughness. I. Direct crack measurements, J. Am. Ceram. Soc. 64 (1981) 533–538.
[18] http://www.ducom.com/.
[19] J. Hanks, Hanks' balanced salt solution and pH control, Methods Cell Sci. 1 (1) (1975) 3–4.
[20] D. Klaffke, Fretting wear of ceramics, Tribol. Int. 22 (2) (1989) 89–101.
[21] J.H. Lee, T. Mori, J.G. Li, T. Ikegami, S. Takenouchi, Impedence spectroscopic estimation of intergranular phase distribution in 15 mol% calcia-stabilized zirconia/alumina composites, J. Eur. Ceram. Soc. 21 (2001) 13–17.
[22] B. Annaz, K.A. Hing, M. Kayser, T. Buckland, L. Di Silvio, Porosity variation in hydroxyapatite and osteoblast morphology: a scanning electron microscopy study, J. Microsc. 215 (2004) 100–110.
[23] M. Kalin, G. Drazic, S. Novak, J. Vizintin, Wear mechanisms associated with the lubrication of zirconia ceramics in various aqueous solutions, J. Eur. Ceram. Soc. 26 (2006) 223–232.
[24] P.Q. Campbell, J.P. Celis, J.R. Roos, O. Van Der Biest, Fretting wear of selected ceramics and cermets, Wear 274 (1994) 47–56.
[25] Y. Sun, B. Li, D. Yang, T. Wang, Y. Sasaki, K. Ishii, Unlubricated friction and wear behaviour of zirconia ceramics, Wear 215 (1998) 232–236.
[26] Y. Wang, F.J. Worzala, A.R. Lefkow, Friction and wear properties of partially stabilized zirconia with solid lubricant, Wear 167 (1993) 23–31.
[27] Y.M. Chen, B. Rigaut, F. Armanet, Wear behaviour of partially stabilized zirconia at high sliding speed, J. Eur. Ceram. Soc. 6 (1990) 383–390.
[28] G.W. Stachowiak, G.B. Stachowiak, Unlubricated friction and wear behaviqur of toughened zirconia ceramics, Wear 132 (1989) 151–171.
[29] G.B. Stachowiak, G.W. Stachowiak, Fretting wear and friction behaviour of engineering ceramics, Wear 190 (1995) 212–218.
[30] R.H.J. Hannink, M.J. Murray, H.G. Scott, Friction and wear of partially stabilized zirconia: basic science and practical applications, Wear 100 (1984) 355–366.
[31] Outokumpu HSC Chemistry® Version 5.1, Outokumpu Research Oy Information Service, P.O. Box 60, FIN-28101, Pori, Finland, 2002, http://www.outokumpu.com/hsc.
[32] V.S. Stubican, S.P. Ray, Phase equilibria and ordering in the system ZrO_2–CaO, J. Am. Ceram. Soc. 60 (1977) 534–537.